
DDoS: DIFFUSION DISTRIBUTION SIMILARITY FOR OUT-OF-DISTRIBUTION DETECTION

Kun Fang¹, Qinghua Tao², Zuopeng Yang³, Xiaolin Huang¹ and Jie Yang¹

¹Department of Automation, Shanghai Jiao Tong University, {fanghenshao, xiaolinhuang, jieyang}@sjtu.edu.cn

²ESAT-STADIUS, KU Leuven, Belgium, qinghua.tao@esat.kuleuven.be

³Guangzhou University, yzpeng44@gmail.com

ABSTRACT

Out-of-Distribution (OoD) detection determines whether the given samples are from the training distribution of the classifier-under-protection, i.e., the In-Distribution (InD), or from a different OoD. Latest researches introduce diffusion models pre-trained on InD data to advocate OoD detection by transferring an OoD image into a generated one that is close to InD, so that one could capture the distribution disparities between original and generated images to detect OoD data. Existing diffusion-based detectors adopt *perceptual metrics* on the two images to measure such disparities, but ignore a fundamental fact: Perceptual metrics are devised essentially for human-perceived similarities of low-level image patterns, e.g., textures and colors, and are *not* advisable in evaluating distribution disparities, since images with different low-level patterns could possibly come from the same distribution. To address this issue, we formulate a diffusion-based detection framework that considers the *distribution similarity* between a tested image and its generated counterpart via a novel proper similarity metric in the informative feature space and probability space learned by the classifier-under-protection. An anomaly-removal strategy is further presented to enlarge such distribution disparities by removing abnormal OoD information in the feature space to facilitate the detection. Extensive empirical results unveil the insufficiency of perceptual metrics and the effectiveness of our distribution similarity framework with new state-of-the-art detection performance.

1 Introduction

Deep Neural Networks (DNNs) hold superior generalization ability on those unseen data that follows the same distribution as that of the training data [1]. However, if DNNs encounter new data that comes from a different distribution in the deployment stage, the output results from DNNs are no longer reliable, which has been a critical issue in those security-sensitive scenarios such as autonomous driving [2]. Generally, the training distribution is known as the In-Distribution \mathbb{P}_{in} (InD), including training and test sets. Samples from other data sets are viewed as Out-of-Distribution (OoD) data. It has been an important research topic in trustworthy deep learning of detecting whether a new sample is from the InD \mathbb{P}_{in} or the OoD \mathbb{P}_{out} of the DNNs, known as the OoD detection problem [3].

Typical non-diffusion OoD detection methods investigate the output logits [4] or features [5] of one given tested image x under a classifier-under-protection to capture disparities between InD and OoD. Recently, latest researches [6, 7, 8] have introduced Diffusion Models (DMs, [9]) into OoD detection due to the powerful ability of DMs in generating high-quality images. Specifically, a DM pre-trained on InD data is available at hand. For any given image x , a *reference* image \hat{x} of x is created through the forward and reverse processes of the DM. As the DM is learned on InD data, the reference image \hat{x} is close to the InD \mathbb{P}_{in} , and thereby an OoD sample x would hold large disparities with its reference \hat{x} . In this way, one could measure the distribution shift from the original x to the reference \hat{x} to detect OoD data.

Existing DMs-based OoD detectors adopt a series of *perceptual metrics* to evaluate the disparities between x and \hat{x} . For example, the LPIPS distance [10] is employed in [6, 7], and the DISTs distance [11] and PSNR are exploited in [8]. Such perceptual metrics mainly focus on the low-level image patterns that can be observed through human eyes,

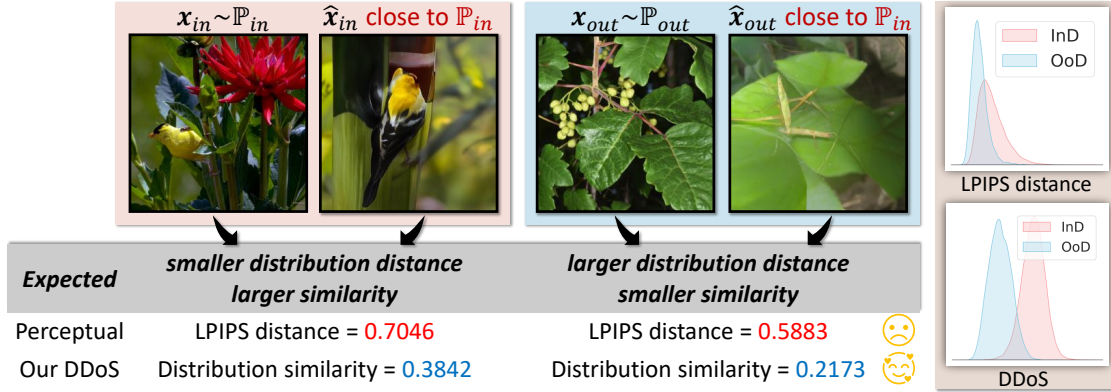


Figure 1: The insufficiency of perceptual metrics in evaluating image similarities for diffusion-based OoD detection. The LPIPS distance assigns inappropriate values for the InD sample x_{in} and OoD sample x_{out} and leads to limited detection results. In contrast, our DDoS well describes the distribution similarity with reasonable scores and substantially improved performance.

e.g., textures, noisy distortions, etc. However, regarding the OoD detection task, the distribution shift between x and \hat{x} actually cannot be well captured through perceptual metrics. A typical case is shown in Fig.1:

- Given an InD image $x_{in} \sim \mathbb{P}_{in}$ and its generated counterpart \hat{x}_{in} , there is supposed to be a small distance between x_{in} and \hat{x}_{in} as they are nearly from the same InD. But, x_{in} and \hat{x}_{in} hold rich and unique image backgrounds and are obviously very different in human-perceived image contents, leading to a large LPIPS distance.
- Meanwhile, a large distance is expected between an OoD image $x_{out} \sim \mathbb{P}_{out}$ and its counterpart \hat{x}_{out} , as \hat{x}_{out} is recovered via a DM pre-trained on InD and thereby close to \mathbb{P}_{in} . But, LPIPS instead allocates a smaller distance for x_{out} and \hat{x}_{out} and views that they are more likely to be similar, which could result from the resembling local structural or textural patterns in x_{out} and \hat{x}_{out} .

In short, such perceptual metrics are devised essentially *not* for deciding whether two images are from the same distribution, and thus lead to limited OoD detection performance.

To evaluate the distribution similarity in two images, not the low-level image patterns but the learned features related to image categories should be considered, which motivates the design of our diffusion-based OoD detection framework, namely **Diffusion Distribution Similarity (DDoS)**. DDoS involves the classifier-under-protection into the framework, so that we can make full use of the informative feature space and probability space learned by the classifier for evaluating distribution similarity. We devise corresponding distribution similarity metrics in the two spaces and leverage their ensemble as the detection score, which well characterizes the distribution shift from x to \hat{x} with reasonable similarity values and improved detection performance, as shown in Fig.1. Besides, an anomaly-removal strategy is executed in the forward procedure of \hat{x} in the classifier-under-protection by removing the abnormal OoD responses in the feature space. This anomaly-removal strategy makes the features and probabilities of the generated \hat{x} more closely approach the InD \mathbb{P}_{in} and even enlarges the distribution shift from an OoD x , which facilitates OoD detection with substantial improvements. Compared with existing supreme DMs-based detection methods [6, 7, 8], our DDoS achieves new state-of-the-art (SOTA) results and verifies the superiority of our distribution similarity metric over the perceptual metric. The contributions of this work are summarized below.

- To address the limitation of perceptual metrics in existing diffusion-based OoD detectors, we propose a detection framework that carefully considers the distribution similarity between a tested image and its diffusion-generated image under the help of the classifier-under-protection.
- The proposed framework includes a distribution similarity metric that thoroughly takes advantage of the probability and feature spaces from the classifier-under-protection, and an anomaly-removal strategy that aims at enlarging the distribution disparities by removing the abnormal OoD information in the feature space.
- Extensive empirical results illustrate the SOTA detection performance of our DDoS detector. Ablation studies and empirical discussions on the involved diffusion model are provided for an in-depth investigation on DDoS.

In the remainder of this paper, Sec.2 outlines the OoD detection problem and the diffusion models. The proposed DDoS detector is thoroughly explained in Sec.3 with the distribution similarity and the anomaly-removal strategy. Extensive empirical results are exhibited in Sec.4. Conclusions and discussions are presented in Sec.5.

2 Related work

2.1 Out-of-distribution detection

Given a new sample $\mathbf{x} \in \mathbb{R}^d$ in the inference stage of the classifier-under-protection, OoD detection is formulated as a bi-classification problem with a decision function $D(\cdot)$ and a scoring function $S(\cdot)$:

$$D(\mathbf{x}) = \begin{cases} \text{InD}, & S(\mathbf{x}) > s, \\ \text{OoD}, & S(\mathbf{x}) < s. \end{cases} \quad (1)$$

If the detection score $S(\mathbf{x})$ is greater than a threshold s , then the decision function $D(\cdot)$ would view \mathbf{x} as an InD sample, and vice versa. The threshold s is selected so that a large fraction of InD samples could be correctly classified. The key to successful OoD detection lies in a suitable $S(\cdot)$ that well describes the disparities between InD and OoD.

Typical *non-diffusion* detection methods leverage distinct information from the given single tested image \mathbf{x} based on the classifier-under-protection, outlined below.

- **Logits-based** detectors try to capture the abnormal responses in the output logits from the classifier-under-protection caused by OoD data. The scoring function can be the maximum probability [12, 13], maximum logits [14, 15] and energy function [4], etc.
- **Features-based** detectors aim at discovering the discrepancy in InD and OoD features, in terms of feature distances [16, 17, 18], feature norms [19] and reconstruction errors [20, 21]. Besides, existing methods also study the anomalous information in features that leads to OoD predictions and try to eliminate such information by ways of truncating features [5, 22, 23, 24].
- **Gradients-based** detectors leverage gradients to distinguish OoD samples from InD samples. For example, the norms of gradients *w.r.t* carefully-devised losses are investigated in [25] for OoD detection. Low-dimensional gradient vectors are learned in [26] to improve the gradient norms.

2.2 Diffusion models for OoD detection

Currently, latest researches make full use of the popular Diffusion Models (DMs), or diffusion denoising probabilistic models [9, 27], to advocate OoD detection. The *forward* and *reverse* processes in DMs are outlined.

- *Forward* process: An image \mathbf{x} is corrupted with T steps of Gaussian noises until it turns into pure noises \mathbf{x}_T :

$$q(\mathbf{x}_t|\mathbf{x}_{t-1}) = \mathcal{N}(\mathbf{x}_t|\sqrt{1-\beta_t}\mathbf{x}_{t-1}, \beta_t\mathbf{I}), \quad (2)$$

where $0 \leq t \leq T$ and β_t follows a fixed variance schedule so that \mathbf{x}_T is close to an isotropic Gaussian $\mathcal{N}(\mathbf{0}, \mathbf{I})$.

- *Reverse* process: A neural network with parameters θ is introduced to remove the noises in \mathbf{x}_T in multiple steps, until a clean image $\hat{\mathbf{x}} = p_\theta(\mathbf{x}_0|\mathbf{x}_T)$ is finally recovered:

$$p_\theta(\mathbf{x}_{t-1}|\mathbf{x}_t) = \mathcal{N}(\mathbf{x}_{t-1}|\mu_\theta(\mathbf{x}_t, t), \Sigma_\theta(\mathbf{x}_t, t)), \quad (3)$$

where μ_θ and Σ_θ are learned mean and variances of Gaussian noises from the neural network θ .

3 Methodology

3.1 Background on diffusion-based detectors

Given a DM with θ pre-trained on InD data and an tested OoD image $\mathbf{x}_{\text{out}} \sim \mathbb{P}_{\text{out}}$, a reference image $\hat{\mathbf{x}}_{\text{out}}$ is created via adding noises on \mathbf{x} and denoising, following the forward and reverse processes above. Since the DM is pre-trained on InD, the recovered image $\hat{\mathbf{x}}$ is certainly close to InD \mathbb{P}_{in} . Clearly, the OoD sample \mathbf{x}_{out} would hold large dissimilarities with its diffusion-generated reference $\hat{\mathbf{x}}_{\text{out}}$, and thus one can try to capture such discrepancy between \mathbf{x} and $\hat{\mathbf{x}}$ for OoD detection.

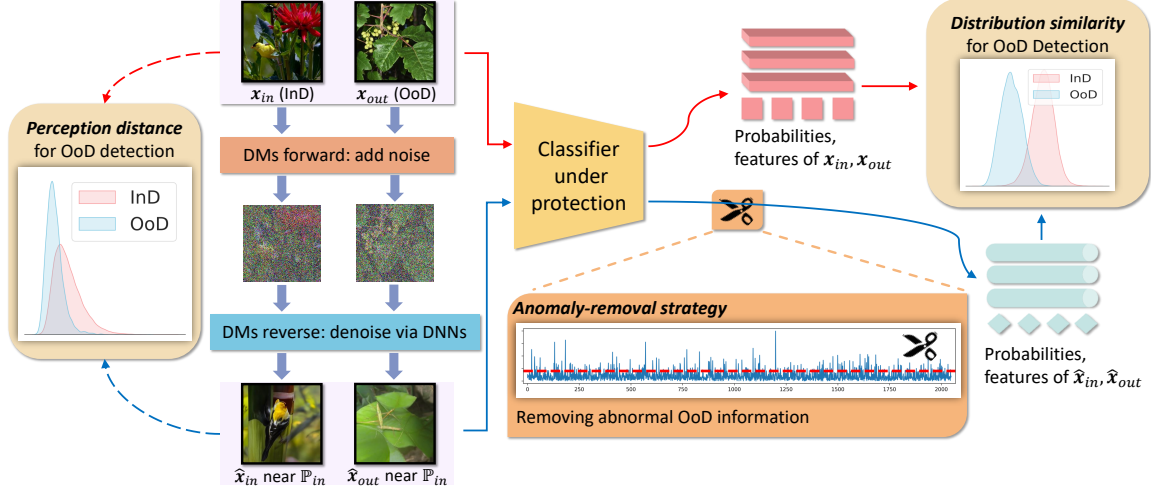


Figure 2: The framework of DDoS. The classifier-under-protection is introduced to calculate the distribution similarity based on the learned feature space and probability space. An anomaly-removal strategy removes the abnormal OoD information for larger distribution disparities with better performance.

A pioneering diffusion-based OoD detector [6] corrupts a clean image x with a range of different noise levels and generates corresponding recovered images \hat{x} . Another method [7] proposes an interesting way by masking x in order to lift it off its distribution, and then employs DMs to inpaint the masked image. A recent work [8] develops multiple test-time techniques in the reverse process of DMs to generate images \hat{x} with larger semantic differences from original images x .

A common point of the aforementioned diffusion-based detection methods [6, 7, 8] is the adopted *perceptual* metric on the tested image x and its DM-generated counterpart \hat{x} , such as LPIPS [10] in [6, 7] and DISTS [11] in [8], to decide whether x is from OoD \mathbb{P}_{out} . Nevertheless, such perceptual distances mainly capture similarities on low-level image patterns, e.g., textures and structures, that can be perceived by human eyes, and are essentially *not* devised for seizing distribution similarities between two images, see an example in Fig.1, which remains to be improved for better detection.

To address the above insufficiency of perceptual metrics, we propose a novel diffusion-based detection framework that involves the classifier-under-protection so as to leverage the informative feature space and probability space to jointly measure the *distribution similarity* between x and \hat{x} . The proposed detection framework is named as **Diffusion Distribution Similarity (DDoS)**, including an effective similarity metric in Sec.3.2 and an anomaly-removal strategy in Sec.3.3, as shown in Fig.2.

3.2 DDoS: Diffusion Distribution Similarity

Suppose an tested image $x \in \mathbb{R}^d$ and its DM-generated $\hat{x} \in \mathbb{R}^d$, the classifier-under-protection $f: \mathbb{R}^d \rightarrow \mathbb{R}^C$ learns penultimate layer features $h_x, h_{\hat{x}} \in \mathbb{R}^m$ and outputs probabilities $g_x, g_{\hat{x}} \in \mathbb{R}^C$ w.r.t C classes. The features $h_x, h_{\hat{x}}$ imply the representations of x, \hat{x} in the latent feature space, and the probabilities $g_x, g_{\hat{x}}$ are obtained by applying a softmax function on the logits of x, \hat{x} .

DDoS on probabilities To measure the distribution similarity in the probability space, we introduce the celebrated Kullback-Leibler (KL) divergence [28] that quantifies the distribution distance between a given probability distribution p and a reference one q :

$$D_{\text{KL}}(p \parallel q) = \sum_i p_i \log \frac{p_i}{q_i}. \quad (4)$$

Accordingly, in the probability space from the classifier-under-protection f , we design a distribution similarity metric on probabilities $g_x, g_{\hat{x}}$ of x, \hat{x} via the KL divergence:

$$\epsilon_{\text{KL}}(x, \hat{x}) = \epsilon_{\text{KL}}(g_x, g_{\hat{x}}) = \frac{D_{\text{KL}}(g_x \parallel u)}{D_{\text{KL}}(g_{\hat{x}} \parallel u)}, \quad (5)$$

with a uniform probability $u = [1/C, \dots, 1/C] \in \mathbb{R}^C$.

Let us take a close look at $\epsilon_{\text{KL}}(\mathbf{x}, \hat{\mathbf{x}})$. Intuitively, the predictive probability of an InD sample is very likely to be concentrated around its ground-truth class, leading to a larger divergence from the uniform probability \mathbf{u} [25]. Consider an OoD sample $\mathbf{x} \sim \mathbb{P}_{\text{out}}$, the KL divergence $D_{\text{KL}}(\mathbf{g}_{\mathbf{x}} \parallel \mathbf{u})$ between the probabilities of \mathbf{x} and the uniform probability \mathbf{u} tends to be small. Meanwhile, for its generated counterpart $\hat{\mathbf{x}}$ that is close to the InD, the KL divergence $D_{\text{KL}}(\mathbf{g}_{\hat{\mathbf{x}}} \parallel \mathbf{u})$ is prone to be large. Accordingly, there exists a smaller value of the similarity $\epsilon_{\text{KL}}(\mathbf{x}, \hat{\mathbf{x}})$ for the OoD sample $\mathbf{x} \sim \mathbb{P}_{\text{out}}$. In this way, $\epsilon_{\text{KL}}(\mathbf{x}, \hat{\mathbf{x}})$ assigns reasonable similarity scores for InD and OoD images, in the probability space from the classifier-under-protection.

Remark We would like to highlight the importance of the uniform probability \mathbf{u} in Eqn.(5), and explain why a direct similarity measurement between $\mathbf{g}_{\mathbf{x}}, \mathbf{g}_{\hat{\mathbf{x}}}$, e.g., $\frac{1}{D_{\text{KL}}(\mathbf{g}_{\hat{\mathbf{x}}} \parallel \mathbf{g}_{\mathbf{x}})}$, is not sensible. Recall the definition of KL divergence in Eqn.(4), p indicates the *observed data distribution* while the reference q represents a *theoretical approximation* of p , and thereby D_{KL} is interpreted as the discrepant information through *using q to model p* . In this sense, as both $\mathbf{g}_{\mathbf{x}}$ and $\mathbf{g}_{\hat{\mathbf{x}}}$ indicate the *observed* probability distributions of InD and OoD, it is unreasonable to apply $\mathbf{g}_{\mathbf{x}}$ and $\mathbf{g}_{\hat{\mathbf{x}}}$ to model each other directly via the KL divergence, and it is justified to introduce a uniform \mathbf{u} as the reference q to approximate the observed predictive probabilities of InD and OoD. Numerical results in Sec.4.3 further validate the ineffectiveness of $\frac{1}{D_{\text{KL}}(\mathbf{g}_{\hat{\mathbf{x}}} \parallel \mathbf{g}_{\mathbf{x}})}$ as the probability similarity metric.

DDoS on features Aside from the similarity metric ϵ_{KL} in the probability space, we further investigate the feature space learned by the classifier-under-protection. Given features $\mathbf{h}_{\mathbf{x}}, \mathbf{h}_{\hat{\mathbf{x}}}$ of \mathbf{x} and its DM-generated counterpart $\hat{\mathbf{x}}$, we consider a simple and effective ℓ_2 distance to measure the feature similarity:

$$\epsilon_{\ell_2}(\mathbf{x}, \hat{\mathbf{x}}) = \epsilon_{\ell_2}(\mathbf{h}_{\mathbf{x}}, \mathbf{h}_{\hat{\mathbf{x}}}) = 1 / \left\| \frac{\mathbf{h}_{\hat{\mathbf{x}}}}{\|\mathbf{h}_{\hat{\mathbf{x}}}\|_2} - \frac{\mathbf{h}_{\mathbf{x}}}{\|\mathbf{h}_{\mathbf{x}}\|_2} \right\|_2. \quad (6)$$

The generated $\hat{\mathbf{x}}$ from DMs of an OoD sample $\mathbf{x} \sim \mathbb{P}_{\text{out}}$ approaches to InD more closely, which implies a large ℓ_2 distance between $\mathbf{h}_{\mathbf{x}}$ and $\mathbf{h}_{\hat{\mathbf{x}}}$ and a small value of the similarity $\epsilon_{\ell_2}(\mathbf{x}, \hat{\mathbf{x}})$ in the feature space. The ℓ_2 -normalization on features $\|\cdot\|_2$ normalizes feature norms and facilitates the ℓ_2 distance in measuring disparities on $\mathbf{h}_{\mathbf{x}}, \mathbf{h}_{\hat{\mathbf{x}}}$, which has been highlighted in [17, 21].

Ensemble By leveraging $\epsilon_{\text{KL}}, \epsilon_{\ell_2}$ in probability and feature spaces, the proposed DDoS well measures the distribution shift of $\hat{\mathbf{x}}$ from \mathbf{x} and thus can serve as an effective detection method. The scoring function of DDoS for OoD detection is devised as an ensemble of ϵ_{KL} and ϵ_{ℓ_2} :

$$S(\mathbf{x}) = \lambda \cdot \epsilon_{\text{KL}}(\mathbf{x}, \hat{\mathbf{x}}) + (1 - \lambda) \cdot \epsilon_{\ell_2}(\mathbf{x}, \hat{\mathbf{x}}). \quad (7)$$

The coefficient $0 \leq \lambda \leq 1$ balances ϵ_{KL} and ϵ_{ℓ_2} .

3.3 An anomaly-removal strategy in DDoS

Recall the key of DDoS: leveraging the distribution disparities between an OoD sample $\mathbf{x} \sim \mathbb{P}_{\text{out}}$ and its DMs-generated counterpart $\hat{\mathbf{x}}$ that is close to InD \mathbb{P}_{in} . Therefore, larger distribution disparities contribute to better detection performance, which motivates the design of an anomaly-removal strategy in DDoS to *enlarge* such disparities.

As the generated $\hat{\mathbf{x}}$ is approaching InD \mathbb{P}_{in} , in the forward procedure of $\hat{\mathbf{x}}$ in the classifier-under-protection f , the peculiar information causing OoD predictions could be removed, so that the outputs of $\hat{\mathbf{x}}$ from f , i.e., features $\mathbf{h}_{\hat{\mathbf{x}}}$ and logits $\mathbf{g}_{\hat{\mathbf{x}}}$, could even reach the InD \mathbb{P}_{in} . In this way, distribution disparities between $\mathbf{h}_{\hat{\mathbf{x}}}, \mathbf{g}_{\hat{\mathbf{x}}}$ and $\mathbf{h}_{\mathbf{x}}, \mathbf{g}_{\mathbf{x}}$ get amplified, which thereby facilitates the detection of an OoD sample $\mathbf{x} \sim \mathbb{P}_{\text{out}}$.

Existing non-diffusion OoD detectors have exploited different ways to eliminate the anomalous OoD information [5, 22, 24, 23]. Generally, the extremely high or low values in the penultimate layer features $\mathbf{h}_{\mathbf{x}}$ are viewed as the abnormal information and should be truncated. Therefore, in our anomaly-removal strategy, we employ the idea of pruning features into our DDoS to remove the peculiar information hidden in the outputs from f of DM-generated $\hat{\mathbf{x}}$, as shown in Fig.2. Particularly, we truncate the learned features $\mathbf{h}_{\hat{\mathbf{x}}}$ via the acknowledged ReAct [5] and VRA [23] techniques due to the cheap computation costs:

$$\mathbf{h}_{\hat{\mathbf{x}}}^{\text{RA}} = \min(\mathbf{h}_{\hat{\mathbf{x}}}, c), \quad \mathbf{h}_{\hat{\mathbf{x}}}^{\text{VRA}} = \begin{cases} 0, & \mathbf{h}_{\hat{\mathbf{x}}} < \alpha, \\ \mathbf{h}_{\hat{\mathbf{x}}}, & \alpha \leq \mathbf{h}_{\hat{\mathbf{x}}} \leq \beta, \\ \beta, & \mathbf{h}_{\hat{\mathbf{x}}} > \beta, \end{cases} \quad (8)$$

where c and α, β , ($\alpha < \beta$) are fixed constants. In this way, the rectified features $\mathbf{h}_{\hat{\mathbf{x}}}^{\text{RA}}, \mathbf{h}_{\hat{\mathbf{x}}}^{\text{VRA}}$ and corresponding probabilities $\mathbf{g}_{\hat{\mathbf{x}}}^{\text{RA}}, \mathbf{g}_{\hat{\mathbf{x}}}^{\text{VRA}}$ of $\hat{\mathbf{x}}$ are more close to the InD \mathbb{P}_{in} , which leads to larger discrepancies from that of an OoD

sample $\mathbf{x} \sim \mathbb{P}_{\text{out}}$ and thus even promotes OoD detection. The final scoring functions of our DDoS and DDoS+ are listed below, *w.r.t* ReAct and VRA:

$$\begin{aligned} S_{\text{DDoS}}(\mathbf{x}) &= \lambda \epsilon_{\text{KL}}(\mathbf{g}_{\mathbf{x}}, \mathbf{g}_{\hat{\mathbf{x}}}^{\text{RA}}) + (1 - \lambda) \epsilon_{\ell_2}(\mathbf{h}_{\mathbf{x}}, \mathbf{h}_{\hat{\mathbf{x}}}^{\text{RA}}), \\ S_{\text{DDoS}+}(\mathbf{x}) &= \lambda \epsilon_{\text{KL}}(\mathbf{g}_{\mathbf{x}}, \mathbf{g}_{\hat{\mathbf{x}}}^{\text{VRA}}) + (1 - \lambda) \epsilon_{\ell_2}(\mathbf{h}_{\mathbf{x}}, \mathbf{h}_{\hat{\mathbf{x}}}^{\text{VRA}}). \end{aligned} \quad (9)$$

Remark We would like to elucidate the novelty of our anomaly-removal strategy differing from those feature-pruning detectors [5, 23]. Despite the same idea of wiping OoD information via feature truncation, the latter is *non-diffusion* and focuses on *one tested image* \mathbf{x} , while ours is executed on *the DM-generated reference image* $\hat{\mathbf{x}}$. Regarding the detection results, the latter further relies on additional logits-based scores, e.g., Energy [4], on the changed logits, while ours directly compares the outputs from the tested \mathbf{x} and its reference $\hat{\mathbf{x}}$ to give detection scores following our devised metric in Eqn.(9). In short, those non-diffusion feature-pruning detectors and our anomaly-removal strategy serve under particular detection frameworks and produce totally different detection scores, where ours maintains superior detection performance, as shown in Sec.4.2.

4 Experiments

Section 4.1 outlines experimental setups. Section 4.2 shows main comparisons with prevailing OoD detectors. Ablation studies on DDoS are performed in Sec.4.3. Section 4.4 gives empirical discussions on the adopted diffusion model in DDoS. *The source code of our work will be released.*

4.1 Setups

Benchmarks Our experiments are based on a prevalent OpenOOD [29] benchmark, which provides a variety of InD and OoD datasets, detectors, checkpoints, etc. In experiments, we only consider the large-scale ImageNet-1K [30] as the InD data, so that the powerful generation ability of diffusion models could be fully exerted on high-resolution images. For the corresponding OoD data, following the settings in [8], 4 datasets are selected from the OpenOOD: Species [31], iNaturalist [32], OpenImage-O [33] and ImageNet-O [34].

- The large-scale ImageNet-1K [30] consists of 1,281,167 training and 50,000 test images from 1,000 categories.
- Species [31] includes both labeled and unlabeled images of invasive species with bounding box annotations. For OoD detection, 10,000 images are sampled by OpenOOD [29].
- iNaturalist [32] contains natural fine-grained images of different species of plants and animals. For OoD detection, 10,000 images are sampled from the selected concepts by OpenOOD [29].
- OpenImage-O [33] is collected image-by-image from the test set of OpenImage-V3. 17,632 images are included in this data set.
- ImageNet-O [34] is gathered from the even large ImageNet-22K data set with ImageNet-1K classes deleted. The 2,000 images in ImageNet-O are even adversarial filtered, and are very hard to be distinguished from the InD ImageNet-1K data.

Image pre-processing In the forward and reverse processes of the diffusion model, the InD and OoD images are resized and cropped to $256 \times 256 \times 3$ and normalized to $[-1, 1]$, following the requirements of the released checkpoints of diffusion models in [35]. Then, in the forward procedure of the classifier-under-protection, the InD and OoD images and their generated counterparts are resized to $224 \times 224 \times 3$ with the mean-variance normalization, as required by the PyTorch-released checkpoints of the classifier-under-protection.

Evaluations Two widely-adopted metrics are calculated to evaluate the detection performance: False Positive Rate (FPR) of OoD samples at a 95% true positive rate of InD samples, and Area Under the Receiver Operating Characteristic Curve (AUROC). Both metrics thoroughly reflect the abilities of detecting OoD samples without misclassifying InD samples for the under-evaluation OoD detectors.

Baselines Two types of baselines are considered:

- *Non-diffusion-based*: MSP [12], ODIN [13], Energy [4], GradNorm [25], ViM [33], KNN [17], MLS [14], ReAct [5] and VRA [23].
- *Diffusion-based*: A pioneering work DDPM [6] detection method and a recent superior one DiffGuard [8], outlined in Sec.2.2.

method	OoD data sets								AVERAGE	
	Species		iNaturalist		OpenImage-O		ImageNet-O			
	FPR↓	AUROC↑	FPR↓	AUROC↑	FPR↓	AUROC↑	FPR↓	AUROC↑	FPR↓	AUROC↑
<i>non-diffusion-based</i>										
MSP	79.52	75.16	52.71	88.42	63.58	84.98	100.00	28.64	73.95	69.30
ODIN	80.89	72.88	50.87	91.14	57.29	89.23	100.00	40.87	72.26	73.53
Energy	82.33	72.04	53.83	90.61	57.10	89.15	100.00	41.91	73.31	73.43
GradNorm	74.42	75.70	26.95	93.87	47.67	85.07	95.60	48.16	61.16	75.70
ReAct	68.65	77.39	19.69	96.37	43.93	90.39	98.00	52.39	57.57	79.13
KNN	76.19	76.38	68.41	85.12	57.56	86.45	84.65	75.37	71.70	80.83
ViM	83.94	70.68	67.85	88.40	57.56	89.63	85.30	70.88	73.66	79.90
MLS	80.87	72.89	50.80	91.15	57.11	89.26	100.00	40.85	72.20	73.54
VRA	69.64	76.94	15.74	97.12	<u>36.42</u>	92.93	95.55	60.79	54.34	81.94
<i>diffusion-based</i>										
DDPM	96.86	44.97	96.27	48.70	94.41	49.35	91.55	51.73	94.77	48.69
DiffGuard	83.68	73.19	71.23	85.81	74.80	82.32	87.74	65.23	79.36	76.64
DiffGuard+KNN	71.04	77.81	48.79	90.19	52.80	87.80	<u>80.85</u>	75.68	63.37	82.87
DiffGuard+ViM	72.26	74.48	39.09	92.50	45.02	91.11	82.30	72.42	59.67	82.63
DiffGuard+MLS	70.31	75.95	30.74	93.03	40.61	90.74	87.05	65.72	57.18	81.36
DDoS	64.81	81.27	10.65	97.89	35.58	<u>92.16</u>	88.05	69.51	49.77	<u>85.20</u>
DDoS+	<u>66.45</u>	<u>81.23</u>	<u>14.67</u>	<u>97.13</u>	41.93	88.70	80.25	<u>75.51</u>	<u>50.82</u>	85.64

Table 1: The detection performance of a variety of OoD detectors (**ResNet50** on **ImageNet-1K**). The **best** and runner-up results are highlighted with bold fonts and underlines, respectively. Our DDoS and DDoS+ achieve new SOTA detection results.

All these strong baselines are *post-hoc* and are directly executed on standard neural networks in inference, without requirements of re-training or structure modifications, see details in Appendix A.

Diffusion models The checkpoints released by OpenAI¹ are adopted [35] and are solely trained on the training set of ImageNet-1K. In the main comparisons of Sec.4.2, we use the conditional 256×256 diffusion model, and adopt the DDIM sampling [36] to accelerate the generation speed. More varied settings on the diffusion model are analysed in Sec.4.4, including unconditional diffusion models and varied sampling timesteps.

We do not consider another popular Latent Diffusion Models (LDMs) [37], as the auto-encoder encoding the latent space of LDMs is trained on a much larger data set than the ImageNet-1K, which implies that the InD of LDMs covers far more data than ImageNet-1K. Therefore, LDMs actually come into conflict with the setups of OoD detection and thus are omitted in experiments.

Classifier-under-protection ResNet50 [38] and DenseNet121 [39] checkpoints pre-trained on ImageNet-1K from PyTorch [40] are employed. See detailed implementation details of DDoS and DDoS+ in Appendix B.

4.2 Main results

Table 1 shows the detection FPR and AUROC values of a variety of non-diffusion-based and diffusion-based methods on each OoD dataset. The diffusion-based DDPM [6] and DiffGuard [8] with perceptual metrics actually manifest much weaker performance than those non-diffusion-based ones. Specifically, DDPM adopts an average of MSE and LPIPS as the detection score, and is reported to be effective only on specific InD and OoD datasets with significant disparities in the original paper, e.g., the human face data set CelebA [41] and the digit data set SVHN [42]. On more complex image sets in Tab.1, DDPM yet shows a complete failure in detecting OoD data from InD data. Another DiffGuard detector with the DISTS distance shows substantial improvements over DDPM for its semantic mismatch-guided techniques in the reverse process of DMs. Even though, DiffGuard has to be combined with other non-diffusion-based detectors in order to achieve competitive results.

In contrast, our DDoS/DDoS+ pays attention to the distribution similarity in feature and probability spaces between the original image and the generated one, which leads to new SOTA detection results with the lowest FPR and highest AUROC values averaged over the OoD datasets. Our empirical findings reveal that the proposed distribution similarity

¹<https://github.com/openai/guided-diffusion>

Method	Score	OoD data sets								AVERAGE	
		Species		iNaturalist		OpenImage-O		ImageNet-O			
		FPR↓	AUROC↑	FPR↓	AUROC↑	FPR↓	AUROC↑	FPR↓	AUROC↑	FPR↓	AUROC↑
DDoS	ϵ_{KL}	85.62	68.52	61.60	88.92	60.05	88.49	100.00	46.10	76.82	73.01
	ϵ_{ℓ_2}	76.45	74.86	29.96	92.95	60.44	77.14	79.65	74.16	61.62	79.78
	Ensemble	64.81	81.27	10.65	97.89	35.58	92.16	88.05	69.51	49.77	85.20
	$\epsilon_{\text{KL-ALT}}$	97.57	49.50	96.93	54.19	98.43	39.70	86.60	66.13	94.88	52.38
	ϵ_{cos}	76.45	74.86	29.96	92.95	60.44	77.14	79.65	74.16	61.62	79.78
DDoS+	Ensemble	84.97	65.09	49.63	85.34	83.52	63.21	78.40	75.32	74.13	72.24
	ϵ_{KL}	87.35	68.28	70.11	86.48	64.58	86.82	99.95	50.94	80.50	73.13
	ϵ_{ℓ_2}	76.45	74.86	29.96	92.95	60.44	77.14	79.65	74.16	61.62	79.78
	Ensemble	66.45	81.23	14.67	97.13	41.93	88.70	80.25	75.51	50.82	85.64
	$\epsilon_{\text{KL-ALT}}$	96.81	51.80	95.09	59.96	97.88	43.78	86.00	67.08	93.95	55.66
DDoS+	ϵ_{cos}	76.45	74.86	29.96	92.95	60.44	77.14	79.65	74.16	61.62	79.78
	Ensemble	82.15	67.69	42.25	88.51	78.43	68.15	77.50	76.40	70.08	75.19

Table 2: The individual and ensemble effects of different alternatives of metrics in the probability space (ϵ_{KL} and $\epsilon_{\text{KL-ALT}}$) and in the feature space (ϵ_{ℓ_2} and ϵ_{cos}).

metric outperforms a broad class of non-diffusion-based detectors and the diffusion-based ones via perceptual distances. Besides, results of DenseNet121 are left to Appendix C.

4.3 Ablation studies

More choices on ϵ_{KL} and ϵ_{ℓ_2} As discussed in Sec.3.2, the similarity ϵ_{KL} on probabilities is devised as a reasonable form of Eqn.(5) based on the definition of the KL divergence in Eqn.(4). We consider another alternative $\epsilon_{\text{KL-ALT}} = 1/D_{\text{KL}}(\mathbf{g}_{\hat{x}}\|\mathbf{g}_x)$ that directly measures disparities in $\mathbf{g}_x, \mathbf{g}_{\hat{x}}$ for comparisons. Besides, aside from the ℓ_2 -distance on features of ϵ_{ℓ_2} in Eqn.(6), we also investigate another option in the feature space: the cosine similarity on features $\epsilon_{\text{cos}} = \frac{\mathbf{h}_{\hat{x}}^\top \mathbf{h}_x}{\|\mathbf{h}_{\hat{x}}\|_2 \|\mathbf{h}_x\|_2}$.

Table 2 shows the individual and ensemble effects of different alternatives on the similarity metric in the probability space (ϵ_{KL} and $\epsilon_{\text{KL-ALT}}$) and the feature space (ϵ_{ℓ_2} and ϵ_{cos}):

- For the probability similarity, $\epsilon_{\text{KL-ALT}}$ falls inferior from ϵ_{KL} , since \mathbf{g}_x and $\mathbf{g}_{\hat{x}}$ are both observed data distributions and cannot be used to model each other as in $\epsilon_{\text{KL-ALT}}$.
- For the feature similarity, both the ℓ_2 distance and the cosine similarity manifest the same detection FPR and AUROC values under DDoS and DDoS+, which possibly due to that the feature clipping and the similarity metric lead to the same order of the final detection scores.

In Tab.2, one can also find that ϵ_{KL} and ϵ_{ℓ_2} individually show limited detection performance. On such basis, the ensemble of the informative probability and feature spaces substantially enhances the OoD detection results, implying the significance of fully leveraging the output information from the classifier-under-protection.

Anomaly-removal on \hat{x} is sufficiently effective The importance of the anomaly-removal strategy in DDoS on the forward procedure of \hat{x} through the classifier f is highlighted in Tab.3. Another three setups about the anomaly-removal strategy are exploited, including DDoS without the removal, DDoS with x removed and DDoS with x, \hat{x} both removed. Among all the four cases, only the devised anomaly-removal strategy on \hat{x} exhibits the best detection performance. Recall that the intuition for the anomaly-removal strategy is to enlarge the disparities between x and \hat{x} where \hat{x} reaches InD more. Such removal cannot be conducted for x since the distribution of x is unknown. Therefore, it is a reasonable way that only the anomalous information from \hat{x} , rather than that from x , could be eliminated.

4.4 Empirical analysis on diffusion models

Conditional v.s. unconditional DMs In the reverse process of DMs, a clean image \hat{x} can be recovered under the guidance of the label information with an additional classifier trained on noisy data [27, 43, 35]. In DDoS, the predicted label from the classifier-under-protection is adopted as the guidance to recover \hat{x} .

Method	Setup	OoD data sets								AVERAGE	
		Species		iNaturalist		OpenImage-O		ImageNet-O		FPR↓	AUROC↑
		FPR↓	AUROC↑	FPR↓	AUROC↑	FPR↓	AUROC↑	FPR↓	AUROC↑		
DDoS	w/o removal	77.74	72.76	47.73	88.65	57.68	85.59	94.20	61.29	69.34	77.07
	Removal on x, \hat{x}	83.07	70.72	74.18	77.32	81.58	70.01	89.95	64.34	82.19	70.60
	Removal on x only	83.48	73.74	77.24	78.57	85.51	66.19	91.45	56.86	84.42	68.84
	Removal on \hat{x} only	64.81	81.27	10.65	97.89	35.58	92.16	88.05	69.51	49.77	85.20
DDoS+	w/o removal	77.74	72.76	47.73	88.65	57.68	85.59	94.20	61.29	69.34	77.07
	Removal on x, \hat{x}	74.34	78.33	36.08	92.71	59.31	81.97	81.00	72.52	62.68	81.38
	Removal on x only	83.11	74.06	74.52	80.73	83.42	68.28	91.20	56.94	83.06	70.00
	Removal on \hat{x} only	66.45	81.23	14.67	97.13	41.93	88.70	80.25	75.51	50.82	85.64

Table 3: Ablation studies on the anomaly-removal strategy of DDoS/DDoS+.

In this section, we consider the effects of unconditional DMs, where \hat{x} is recovered without any label information. Empirical results in Tab.4 indicate that DDoS with unconditional DMs falls inferior from DDoS with conditional DMs. The reasons behind possibly lie in that the generated \hat{x} with the label guidance approaches more closely towards the InD \mathbb{P}_{in} than those without the label guidance, contributing to a more significant distribution disparity between the original x and the reference \hat{x} with improved OoD detection performance.

Method	DMs	OoD data sets								AVERAGE	
		Species		iNaturalist		OpenImage-O		ImageNet-O		FPR↓	AUROC↑
		FPR↓	AUROC↑	FPR↓	AUROC↑	FPR↓	AUROC↑	FPR↓	AUROC↑		
DDoS	uncond.	68.44	79.43	13.26	97.50	40.56	90.00	90.95	63.82	53.30	82.69
	cond.	64.81	81.27	10.65	97.89	35.58	92.16	88.05	69.51	49.77	85.20
DDoS+	uncond.	73.38	75.75	19.41	95.89	49.13	84.00	85.50	68.51	56.86	81.04
	cond.	66.45	81.23	14.67	97.13	41.93	88.70	80.25	75.51	50.82	85.64

Table 4: Comparisons on unconditional and conditional DMs in DDoS/DDoS+.

Effect of varied diffusion timesteps DDoS adopts the DDIM sampling [36] in the diffusion model, so as for fewer sampling steps T in the reverse processes. Different steps T significantly affect the quality of generated images \hat{x} , and thereby influence the detection performance. A wide range of different values for the diffusion timesteps T are exploited for a sensitivity analysis on the detection results of DDoS, shown in Fig.3. Generally, as the diffusion timestep T increases, the detection results get improved accordingly, since the quality of the recovered image \hat{x} also gets enhanced. DDoS adopts a default value of $T = 24$ following the recommended settings in [35].

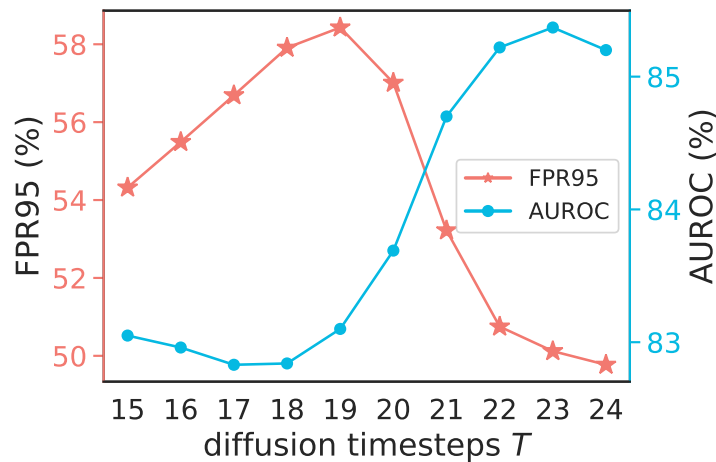


Figure 3: The average detection FPR and AUROC on multiple OoD datasets w.r.t varied diffusion timesteps T of DDoS.

5 Conclusion and discussion

The proposed DDoS framework addresses the drawback of perceptual metrics in characterizing the distribution shift between two images, and significantly advocates the diffusion-based OoD detection methods with substantially enhanced detection performance. A novel distribution similarity metric is based on the probability and feature spaces from the classifier-under-protection through the well-known KL divergence and the ℓ_2 distance, respectively. An anomaly-removal strategy is executed on the forward procedure of the generated image in the classifier-under-protection by removing the OoD abnormal information to enlarge the distribution disparities between the original and the generated images. In this way, the distribution shift between an OoD image and its diffusion-generated counterpart gets well captured by DDoS, leading to new SOTA detection results.

In addition, the limitation of this work mainly lies in the extra memory costs of the diffusion model and the time-consuming of the reverse process, which is also a common limitation of diffusion-based OoD detectors. One could mitigate such issues by introducing advanced techniques in diffusion models, such as lightweight model checkpoints and faster sampling schedules. Another pre-requisite of DDoS is that the DM and classifier-under-protection should be sufficiently trained on InD data, as unconfident DM and classifier-under-protection on InD data might lead to generated images with limited qualities and unreliable features and biased probabilities, hurting the detection performance.

References

- [1] Yann LeCun, Yoshua Bengio, and Geoffrey Hinton. Deep learning. *nature*, 521(7553):436–444, 2015.
- [2] Vikash Schwag, Arjun Nitin Bhagoji, Liwei Song, Chawin Sitawarin, Daniel Cullina, Mung Chiang, and Prateek Mittal. Analyzing the robustness of open-world machine learning. In *Proceedings of the 12th ACM Workshop on Artificial Intelligence and Security*, pages 105–116, 2019.
- [3] Jingkang Yang, Kaiyang Zhou, Yixuan Li, and Ziwei Liu. Generalized out-of-distribution detection: A survey. *International Journal of Computer Vision*, pages 1–28, 2024.
- [4] Weitang Liu, Xiaoyun Wang, John Owens, and Yixuan Li. Energy-based out-of-distribution detection. *Advances in neural information processing systems*, 33:21464–21475, 2020.
- [5] Yiyu Sun, Chuan Guo, and Yixuan Li. React: Out-of-distribution detection with rectified activations. *Advances in Neural Information Processing Systems*, 34:144–157, 2021.
- [6] Mark S Graham, Walter HL Pinaya, Petru-Daniel Tudosiu, Parashkev Nachev, Sebastien Ourselin, and M Jorge Cardoso. Denoising diffusion models for out-of-distribution detection. In *2023 IEEE/CVF Conference on Computer Vision and Pattern Recognition Workshops (CVPRW)*, pages 2948–2957. IEEE, 2023.
- [7] Zhenzhen Liu, Jin Peng Zhou, Yufan Wang, and Kilian Q Weinberger. Unsupervised out-of-distribution detection with diffusion inpainting. In *International Conference on Machine Learning*, pages 22528–22538. PMLR, 2023.
- [8] Ruiyuan Gao, Chenchen Zhao, Lanqing Hong, and Qiang Xu. Diffguard: Semantic mismatch-guided out-of-distribution detection using pre-trained diffusion models. In *Proceedings of the IEEE/CVF International Conference on Computer Vision*, pages 1579–1589, 2023.
- [9] Jonathan Ho, Ajay Jain, and Pieter Abbeel. Denoising diffusion probabilistic models. *Advances in neural information processing systems*, 33:6840–6851, 2020.
- [10] Richard Zhang, Phillip Isola, Alexei A Efros, Eli Shechtman, and Oliver Wang. The unreasonable effectiveness of deep features as a perceptual metric. In *Proceedings of the IEEE conference on computer vision and pattern recognition*, pages 586–595, 2018.
- [11] Keyan Ding, Kede Ma, Shiqi Wang, and Eero P Simoncelli. Image quality assessment: Unifying structure and texture similarity. *IEEE transactions on pattern analysis and machine intelligence*, 44(5):2567–2581, 2020.
- [12] Dan Hendrycks and Kevin Gimpel. A baseline for detecting misclassified and out-of-distribution examples in neural networks. In *International Conference on Learning Representations*, 2016.
- [13] Shiyu Liang, Yixuan Li, and R Srikant. Enhancing the reliability of out-of-distribution image detection in neural networks. In *International Conference on Learning Representations*, 2018.
- [14] Dan Hendrycks, Steven Basart, Mantas Mazeika, Andy Zou, Joseph Kwon, Mohammadreza Mostajabi, Jacob Steinhardt, and Dawn Song. Scaling out-of-distribution detection for real-world settings. In *International Conference on Machine Learning*, pages 8759–8773. PMLR, 2022.
- [15] Zihan Zhang and Xiang Xiang. Decoupling maxlogit for out-of-distribution detection. In *Proceedings of the IEEE/CVF Conference on Computer Vision and Pattern Recognition*, pages 3388–3397, 2023.

- [16] Kimin Lee, Kibok Lee, Honglak Lee, and Jinwoo Shin. A simple unified framework for detecting out-of-distribution samples and adversarial attacks. *Advances in neural information processing systems*, 31, 2018.
- [17] Yiyu Sun, Yifei Ming, Xiaojin Zhu, and Yixuan Li. Out-of-distribution detection with deep nearest neighbors. In *International Conference on Machine Learning*, pages 20827–20840. PMLR, 2022.
- [18] Jaewoo Park, Yoon Gyo Jung, and Andrew Beng Jin Teoh. Nearest neighbor guidance for out-of-distribution detection. In *Proceedings of the IEEE/CVF International Conference on Computer Vision*, pages 1686–1695, 2023.
- [19] Yeonguk Yu, Sungho Shin, Seongju Lee, Changhyun Jun, and Kyoobin Lee. Block selection method for using feature norm in out-of-distribution detection. In *Proceedings of the IEEE/CVF Conference on Computer Vision and Pattern Recognition*, pages 15701–15711, 2023.
- [20] Xiaoyuan Guan, Zhouwu Liu, Wei-Shi Zheng, Yuren Zhou, and Ruixuan Wang. Revisit pca-based technique for out-of-distribution detection. In *Proceedings of the IEEE/CVF International Conference on Computer Vision*, pages 19431–19439, 2023.
- [21] Kun Fang, Qinghua Tao, Kexin Lv, Mingzhen He, Xiaolin Huang, and Jie Yang. Kernel pca for out-of-distribution detection. *arXiv preprint arXiv:2402.02949*, 2024.
- [22] Yao Zhu, YueFeng Chen, Chuanlong Xie, Xiaodan Li, Rong Zhang, Hui Xue, Xiang Tian, Yaowu Chen, et al. Boosting out-of-distribution detection with typical features. *Advances in Neural Information Processing Systems*, 35:20758–20769, 2022.
- [23] Mingyu Xu, Zheng Lian, Bin Liu, and Jianhua Tao. Vra: Variational rectified activation for out-of-distribution detection. *Advances in Neural Information Processing Systems*, 36:28941–28959, 2023.
- [24] Yue Song, Nicu Sebe, and Wei Wang. Rankfeat: Rank-1 feature removal for out-of-distribution detection. *Advances in Neural Information Processing Systems*, 35:17885–17898, 2022.
- [25] Rui Huang, Andrew Geng, and Yixuan Li. On the importance of gradients for detecting distributional shifts in the wild. *Advances in Neural Information Processing Systems*, 34:677–689, 2021.
- [26] Yingwen Wu, Tao Li, Xinwen Cheng, Jie Yang, and Xiaolin Huang. Low-dimensional gradient helps out-of-distribution detection. *arXiv preprint arXiv:2310.17163*, 2023.
- [27] Jascha Sohl-Dickstein, Eric Weiss, Niru Maheswaranathan, and Surya Ganguli. Deep unsupervised learning using nonequilibrium thermodynamics. In *International conference on machine learning*, pages 2256–2265. PMLR, 2015.
- [28] Solomon Kullback and Richard A Leibler. On information and sufficiency. *The annals of mathematical statistics*, 22(1):79–86, 1951.
- [29] Jingkan Yang, Pengyun Wang, Dejian Zou, Zitang Zhou, Kunyuan Ding, Wenxuan Peng, Haoqi Wang, Guangyao Chen, Bo Li, Yiyu Sun, et al. Openood: Benchmarking generalized out-of-distribution detection. *Advances in Neural Information Processing Systems*, 35:32598–32611, 2022.
- [30] Jia Deng, Wei Dong, Richard Socher, Li-Jia Li, Kai Li, and Li Fei-Fei. Imagenet: A large-scale hierarchical image database. In *IEEE Conference on Computer Vision and Pattern Recognition*, pages 248–255, 2009.
- [31] Wei He, Kai Han, Ying Nie, Chengcheng Wang, and Yunhe Wang. Species196: A one-million semi-supervised dataset for fine-grained species recognition. *Advances in Neural Information Processing Systems*, 36, 2024.
- [32] Grant Van Horn, Oisin Mac Aodha, Yang Song, Yin Cui, Chen Sun, Alex Shepard, Hartwig Adam, Pietro Perona, and Serge Belongie. The inaturalist species classification and detection dataset. In *Proceedings of the IEEE conference on computer vision and pattern recognition*, pages 8769–8778, 2018.
- [33] Haoqi Wang, Zhizhong Li, Litong Feng, and Wayne Zhang. Vim: Out-of-distribution with virtual-logit matching. In *Proceedings of the IEEE/CVF Conference on Computer Vision and Pattern Recognition*, pages 4921–4930, 2022.
- [34] Dan Hendrycks, Kevin Zhao, Steven Basart, Jacob Steinhardt, and Dawn Song. Natural adversarial examples. In *Proceedings of the IEEE/CVF conference on computer vision and pattern recognition*, pages 15262–15271, 2021.
- [35] Prafulla Dhariwal and Alexander Nichol. Diffusion models beat gans on image synthesis. *Advances in neural information processing systems*, 34:8780–8794, 2021.
- [36] Jiaming Song, Chenlin Meng, and Stefano Ermon. Denoising diffusion implicit models. In *International Conference on Learning Representations*, 2020.

- [37] Robin Rombach, Andreas Blattmann, Dominik Lorenz, Patrick Esser, and Björn Ommer. High-resolution image synthesis with latent diffusion models. In Proceedings of the IEEE/CVF conference on computer vision and pattern recognition, pages 10684–10695, 2022.
- [38] Kaiming He, Xiangyu Zhang, Shaoqing Ren, and Jian Sun. Deep residual learning for image recognition. In IEEE Conference on Computer Vision and Pattern Recognition, pages 770–778, 2016.
- [39] Gao Huang, Zhuang Liu, Laurens Van Der Maaten, and Kilian Q Weinberger. Densely connected convolutional networks. In Proceedings of the IEEE conference on computer vision and pattern recognition, pages 4700–4708, 2017.
- [40] Adam Paszke, Sam Gross, Francisco Massa, Adam Lerer, James Bradbury, Gregory Chanan, Trevor Killeen, Zeming Lin, Natalia Gimelshein, Luca Antiga, et al. Pytorch: An imperative style, high-performance deep learning library. Advances in neural information processing systems, 32, 2019.
- [41] Ziwei Liu, Ping Luo, Xiaogang Wang, and Xiaoou Tang. Deep learning face attributes in the wild. In Proceedings of the IEEE international conference on computer vision, pages 3730–3738, 2015.
- [42] Yuval Netzer, Tao Wang, Adam Coates, Alessandro Bissacco, Bo Wu, and Andrew Y Ng. Reading digits in natural images with unsupervised feature learning. In Proceedings of the NIPS Workshop on Deep Learning and Unsupervised Feature Learning, 2011.
- [43] Yang Song, Jascha Sohl-Dickstein, Diederik P Kingma, Abhishek Kumar, Stefano Ermon, and Ben Poole. Score-based generative modeling through stochastic differential equations. In International Conference on Learning Representations, 2020.

Appendix A Details of the baseline OoD detectors

We elaborate the details of the scoring functions $S(\cdot)$ of the non-diffusion-based OoD detectors involved in experiments, covering three different types of logits-, gradients-, and features-based methods.

The classifier-under-protection $f : \mathbb{R}^d \rightarrow \mathbb{R}^C$ learns features $\mathbf{h}_x \in \mathbb{R}^m$ before the last linear layer and outputs predictive logits $\bar{\mathbf{g}}_x = f(\mathbf{x}) \in \mathbb{R}^C$ of the inputs $\mathbf{x} \in \mathbb{R}^d$. Notice that the probabilities \mathbf{g}_x in the main text are obtained by apply a softmax function on the logits $\bar{\mathbf{g}}_x$.

MSP [12] MSP takes the maximum value of probabilities of \mathbf{x} from the classifier-under-protection as the scoring function:

$$S_{\text{MSP}}(\mathbf{x}) = \max(\text{softmax}(\bar{\mathbf{g}}_x)) = \max(\mathbf{g}_x). \quad (10)$$

ODIN [13] ODIN improves MSP by applying temperature scaling on the logits of the adversarial examples of \mathbf{x} :

$$S_{\text{ODIN}}(\mathbf{x}) = \max(\text{softmax}(\frac{f(\mathbf{x}_{adv})}{T})). \quad (11)$$

\mathbf{x}_{adv} denotes the adversarial examples of \mathbf{x} , and T indicates the temperature coefficient.

Energy [4] Energy applies the energy function on the logits $\bar{\mathbf{g}}_x$ of the inputs \mathbf{x} from the classifier-under-protection. The analysis [41] shows that energy is well aligned with the input probability density.

$$S_{\text{Energy}}(\mathbf{x}) = \log \sum_{i=1}^C \exp(\bar{\mathbf{g}}_x[i]), \quad (12)$$

where $\bar{\mathbf{g}}_x[i]$ denotes the i -th element in logits $\bar{\mathbf{g}}_x \in \mathbb{R}^C$.

GradNorm [25] GradNorm proposes a novel loss as the KL divergence between the probabilities of \mathbf{x} and a uniform distribution $\mathbf{u} = [1/C, \dots, 1/C] \in \mathbb{R}^C$, and then take the gradients *w.r.t* this loss on the weight parameter $\mathbf{W} \in \mathbb{R}^{m \times C}$ of the last linear layer in the classifier-under-protection. The ℓ_1 norm of the gradients is verified as an effective detection score:

$$S_{\text{GradNorm}}(\mathbf{x}) = \left\| \frac{\partial \text{KL}(\mathbf{g}_x \parallel \mathbf{u})}{\partial \mathbf{W}} \right\|_1. \quad (13)$$

ViM [33] ViM combines the logits and features together from the classifier-under-protection for OoD detection. Firstly, all the training features are gathered and the residual subspace is extracted by PCA. Then, in the inference stage, the features \mathbf{h}_x of a new sample \mathbf{x} is projected to the residual space, and the norm of the projected feature is computed. After that, the projected feature norm is put as an additional dimension in the logits $\bar{\mathbf{g}}_x$, and the extended logits get normalized via the softmax function. Finally, the value of the normalized projected feature norm is set as the detection score.

KNN [17] KNN is a simple and effective OoD detection method also with significantly heavy memory and time costs, as all the N_{tr} training features have to be stored and iterated. The nearest neighbor searching is executed between the features of the new sample and all the features of the training data. The negative of the (k -th) shortest ℓ_2 distance is set as the detection score:

$$S_{\text{KNN}}(\mathbf{x}) = - \min_{i:1, \dots, N_{\text{tr}}} \left\| \frac{\mathbf{h}_x}{\|\mathbf{h}_x\|_2} - \frac{\mathbf{h}_{\mathbf{x}_{\text{tr}}}^i}{\|\mathbf{h}_{\mathbf{x}_{\text{tr}}}^i\|_2} \right\|_2. \quad (14)$$

$\mathbf{h}_{\mathbf{x}_{\text{tr}}}^i$ denotes features of the i -th training sample.

MLS [14] MLS claims that the classic MSP does not well scale to large-scale challenging data sets, and instead proposes that the maximum logits are superior in large-scale and multi-class anomaly segmentation:

$$S_{\text{MLS}}(\mathbf{x}) = \max(\bar{\mathbf{g}}_x). \quad (15)$$

method	OoD data sets								AVERAGE	
	Species		iNaturalist		OpenImage-O		ImageNet-O			
	FPR↓	AUROC↑	FPR↓	AUROC↑	FPR↓	AUROC↑	FPR↓	AUROC↑	FPR↓	AUROC↑
<i>non-diffusion-based</i>										
MSP	80.29	74.75	49.28	89.05	66.80	83.83	98.65	47.39	73.76	73.76
ODIN	79.59	72.56	39.57	92.81	57.65	88.49	97.50	56.41	68.58	77.57
Energy	80.25	71.66	39.70	92.66	56.51	88.49	96.45	57.46	68.23	77.57
GradNorm	79.35	69.36	26.70	93.40	55.27	80.66	92.35	54.68	63.42	74.53
ReAct	77.64	77.65	46.87	90.30	67.97	73.93	93.00	48.35	71.37	72.56
KNN	85.77	73.58	86.52	74.91	67.26	81.03	69.85	81.64	77.35	77.79
MLS	79.59	72.56	39.58	92.81	57.63	88.49	97.50	56.40	68.58	77.57
VRA	76.00	75.05	33.71	93.05	55.29	82.49	85.00	63.74	62.5	78.58
<i>diffusion-based</i>										
DDPM	96.86	44.97	96.27	48.70	94.41	49.35	91.55	51.73	94.77	48.69
DDoS	<u>75.55</u>	<u>75.08</u>	<u>20.13</u>	<u>96.19</u>	<u>44.95</u>	<u>88.82</u>	<u>74.55</u>	<u>79.20</u>	<u>53.79</u>	84.82
DDoS+	75.42	72.10	19.07	96.37	40.68	90.98	77.95	76.53	53.28	<u>83.99</u>

Table 5: The detection performance of various OoD detectors (**DenseNet121** on **ImageNet-1K**). The **best** and runner-up results are highlighted with bold fonts and underlines, respectively. Our DDoS/DDoS+ achieve new SOTA detection results.

Appendix B Implementation details of DDoS and DDoS+

In the part of image synthesis via diffusion models, DDoS and DDoS+ adopt the recommended settings in [35], see detailed hyper-parameters of diffusion models in both the released code of [35] and ours.

In the part of the boosting strategy of DDoS and DDoS+, for the ReAct in DDoS, the threshold c in Eqn.(8) is specified as $c = 0.1$ to acquire the features $h_{\hat{x}}^{\text{ReAct}}$ and logits $g_{\hat{x}}^{\text{ReAct}}$ for both ResNet50 and DenseNet121. For the VRA in DDoS+, the features $h_{\hat{x}}^{\text{VRA}}$ are kept the same as $h_{\hat{x}}^{\text{ReAct}}$, and the thresholds α, β in Eqn.(8) are specified as $\alpha = 0.1, \beta = 0.5$ to obtain the logits $g_{\hat{x}}^{\text{VRA}}$ for ResNet50 and $\alpha = 0.1, \beta = 0.2$ for DenseNet121.

In the part of the ensemble of DDoS and DDoS+ in Eqn.(7), the similarities $\epsilon_{\text{KL}}, \epsilon_{\ell_2}$ from logits and features belong to different orders of magnitude. Therefore, ϵ_{KL} and ϵ_{ℓ_2} are supposed to be normalized before the ensemble. To be specific, we adopt the min-max normalization on ϵ_{KL} and ϵ_{ℓ_2} with the maximum and minimum values of the available InD data, respectively. In addition, the coefficient λ in ensemble is specified as $\lambda = 0.5$ for DDoS, $\lambda = 0.45$ for DDoS+ of ResNet50 and $\lambda = 0.65$ for DDoS+ of DenseNet121.

Regarding the GPU resources, experiments for the image synthesis via diffusion models are executed parallelly on 4 NVIDIA v100 GPUs, and experiments for the forward procedure in the classifier-under-protection are executed on 1 NVIDIA GeForce RTX 3090 GPU.

Appendix C Main results on DenseNet121

Table 5 illustrates the comparison detection results with the classifier-under-protection of DenseNet121 trained on ImageNet-1K as the InD data. Our DDoS and DDoS+ keep superior detection performance on DenseNet121 over other non-diffusion-based and diffusion-based OoD detectors with lowest FPR and high AUROC values averaged on the OoD data sets. The DDPM detector [6] does not rely on the classifier-under-protection and thus shows the same detection performance as that of ResNet50. We are unable to reproduce DiffGuard [8] on DenseNet121 based on the released code and have to omit the comparison here. Table 5 and Tab.1 in the main text together validate the effectiveness of our distribution similarity metric in diffusion-based detection.